frontiers | Frontiers in Astronomy and Space Sciences

TYPE Original Research
PUBLISHED 07 October 2022
DOI 10.3389/fspas.2022.994980

OPEN ACCESS

EDITED BY
Samuel Andrea Giuliani,
Universidad Autónoma de Madrid, Spain

REVIEWED BY
Athanasios Psaltis,
Darmstadt University of Technology, Germany
Igor Panov,
Kurchatov Institute, Russia

*CORRESPONDENCE
Diego Vescovi,
vescovi@iap.uni-frankfurt.de

SPECIALTY SECTION
This article was submitted to Nuclear Physics,
a section of the journal
Frontiers in Astronomy and Space Sciences

RECEIVED 15 July 2022
ACCEPTED 08 September 2022
PUBLISHED 07 October 2022

CITATION
Vescovi D, Reifarth R, Cristallo S and Couture A (2022), Neutron-capture measurement candidates for the r-process in neutron star mergers. *Front. Astron. Space Sci.* 9:994980. doi: 10.3389/fspas.2022.994980

Neutron-capture measurement candidates for the r-process in neutron star mergers

Diego Vescovi[1]*, René Reifarth[1], Sergio Cristallo[2,3] and Aaron Couture[4]

[1]Institute for Applied Physics, Goethe University Frankfurt, Frankfurt, Germany, [2]INAF—Osservatorio Astrofisico D'Abruzzo, Teramo, Italy, [3]INFN—Sezione di Perugia, Perugia, Italy, [4]Los Alamos National Laboratory, Los Alamos, NM, United States

Neutron star mergers (NSMs) are one of the astrophysical sites for the occurrence of the rapid neutron capture process (r-process). After a merger, the ejected neutron-rich matter hosts the production of radioactive heavy nuclei located far from the stability valley. Their nuclear physics properties are key inputs for r-process nucleosynthesis calculations. Here, we focus on the importance of neutron-capture rates and perform a sensitivity study for typical outflows from NSMs. We identify the rates with the highest impact on the final r-process abundance pattern and the nuclear energy release, therefore determining the nucleosynthesis in NSMs. A list of major n-capture rates affecting individual isotopes and elements production is also provided.

KEYWORDS

neutron stars, compact binary mergers, gravitational waves, multimessenger astrophysics, kilonovae, r-process, neutron - nuclear reactions

1 Introduction

Elements heavier than iron are mainly synthesized, to a nearly equal proportion, through the slow neutron capture process (s-process) (Käppeler et al., 2011) and the rapid neutron capture process (r-process) (Cowan et al., 2021). One of the most challenging problems in current nuclear physics and astrophysics is identifying the astrophysical r-process sites. The production of r-process nuclei requires very high neutron densities ($n_n > 10^{20}$ cm^{-3}) and temperatures ($T > 10^9$ K). Therefore, the most obvious candidates are explosive events involving either the collapse of single massive stars or the merger of compact remnants such as binary neutron star (BNS) or black hole (BH)-neutron star (BHNS) systems.

In compact binary merger (CBM) systems, energy is released through the emission of gravitational waves. As a consequence, the loss of energy gradually makes the binary orbit to shrink, and the inspiral of the two compact objects ends with their merger. Numerical simulations show that, during the last phase of the coalescence, the matter is dynamically ejected on timescales of milliseconds into two components: a cold and very neutron-rich (electron fraction $Y_e \sim 0.1$) tidal ejecta mainly distributed on the orbital plane (equatorial angles) and a more isotropic shock-heated ejecta originating from the contact interface between the two objects. The former can be observed both in BNS and BHNS systems and

is constituted by material from the tidal disruption of the neutron star. The latter is typically associated with a BNS system. In this case, the *dynamical ejecta*, especially at high latitudes (polar angles), is subject to pair processes and neutrino irradiation from the central remnant, which increase Y_e up to ~ 0.4 [see Radice et al. (2020), for a review]. From the merger, either a prompt formation of a BH or of a massive neutron star (MNS), which survives for a short time before collapsing in turn into a BH, can occur. Around the merger remnant, an accretion disk is formed, from which material can be ejected again in the form of wind. The main ejection mechanisms of the disk are the deposition of neutrinos emitted from the surface of the central body, viscous friction, and α-recombination. The *neutrino-driven wind* is ejected mainly in the polar direction and is moderately neutron-rich ($Y_e \gtrsim 0.25$) (Perego et al., 2014). The *viscous-driven wind* is launched in the equatorial direction and contains up to 40% of the disk mass with a Y_e distribution in the range 0.1–0.4, depending on the lifetime of the MNS (Lippuner et al., 2017; Fujibayashi et al., 2018). This ejecta is thought to constitute the bulk of the outflow (Radice et al., 2020). Additional fast disk winds may also be driven by magnetic processes (*magnetically-driven wind*) (Metzger et al., 2018; Ciolfi and Kalinani, 2020; Shibata et al., 2021) or spiral wave triggered by $m = 1$ spiral modes in the long-lived MNS remnant (*spiral-wave wind*) (Nedora et al., 2019, 2021) and are characterized by electron fraction typically larger than ~ 0.25.

Short gamma-ray burst and kilonova emission are typical electromagnetic signals associated with CBMs [see Metzger (2019), for a review]. In BNS mergers, the neutron-rich matter is ejected through various channels and, as it expands into space, hosts the production of r-process nuclei, whose radioactive decay heats the ejecta. The ensuing radiation eventually emerges from the optically-thick ejecta and powers an electromagnetic transient known as *kilonova*. The first phenomenon of this kind to be observed was the electromagnetic counterpart AT2017gfo (Arcavi et al., 2017; Coulter et al., 2017; Drout et al., 2017; Evans et al., 2017; Kasliwal et al., 2017; Nicholl et al., 2017; Pian et al., 2017; Smartt et al., 2017; Soares-Santos et al., 2017; Tanvir et al., 2017) of the gravitational wave detection GW170817 of a BNS merger (Abbott et al., 2017a,b). The fair agreement of the luminosity and bolometric light curve evolution of AT2017gfo to kilonova models considering the heating rate and opacity expected from freshly synthesized r-process elements (Kasen et al., 2017; Perego et al., 2017; Villar et al., 2017; Tanaka et al., 2017; Wollaeger et al., 2018; Watson et al., 2019; Gillanders et al., 2022), provided the first direct indication that the r-process elements are actually produced in neutron star mergers (NSMs).

During the r-process nucleosynthesis in NSM ejecta, the attained neutron fluxes are so high to cause unstable neutron-rich nuclei, located along the dripline, to be rapidly synthesized, possibly also populating the region in which nuclear fission is extremely efficient. The early r-process is characterized by (n, γ) $\rightleftarrows$ (γ, n) equilibrium, with neutron capture on heavy nuclei proceeding much faster than β-decay (Arcones and Martínez-Pinedo, 2011). During this early phase, the isotope abundances depend on the temperature, the neutron abundance, and the neutron separation energies. The latter is determined by nuclear masses, and so by the nuclear-mass model considered for these unstable heavy nuclei (Sprouse et al., 2020). At some point, however, the availability of free neutrons is drastically reduced and a freeze-out occurs. This happens when the neutron-to-seed ratio, namely the neutrons captured per seed nucleus, drops below unity. After freeze-out, the equilibrium is no longer maintained and competition between neutron captures, photodissociations, β-decay, and β-delayed neutron emission arises. The interplay between them shapes the final abundance distribution of heavy elements, and the nuclear heating rate powering the possible electromagnetic transients associated with the r-process astrophysical scenarios.

Within this framework, knowing the nuclear properties of neutron-rich unstable nuclei, such as nuclear masses, β-decay rates, neutron-capture rates, and fission fragment distributions [see, e.g., Mumpower et al. (2016), Kullmann et al. (2022)], is crucial for r-process nucleosynthesis calculations. Unfortunately, for most of these nuclei, they are poorly known, and we have to rely on theoretical models, whose predictions can largely vary, depending on the assumptions made (Horowitz et al., 2019). This is particularly true for neutron-capture rates, whose direct experimental measurements are currently unfeasible. The half-life limit for direct measurements using current facilities is typically a few years (Couture and Reifarth, 2007; Reifarth et al., 2018). Capture cross sections of isotopes with shorter half-lives can only be investigated indirectly (Reifarth et al., 2014) or have to be based on theoretical estimates.

In this respect, next-generation neutron facilities might make the production and the study of many exotic nuclei accessible, thus providing key nuclear information of interest for r-process studies (Reifarth and Litvinov, 2014; Reifarth et al., 2017).

As a matter of fact, the theoretical rates determined using the Hauser–Feshbach (HF) statistical model (Hauser and Feshbach, 1952) are very often the sole option. However, variations by over two to three orders of magnitudes are predicted, depending on the different choices for nuclear structure properties, optical potentials, level densities, and γ-ray strengths of nuclei located far from the beta stability valley [see, e.g., Arnould et al. (2007)].

Sensitivity studies aiming at determining the impact of nuclear physics uncertainties on abundance predictions for astrophysical model conditions suitable to produce the weak and the main r-process components were performed in the past [e.g., Surman et al. (2009); Mumpower et al. (2012); Surman et al. (2014); Mumpower et al. (2016)]. More recently, uncertainties arising from different adopted mass models, spontaneous fission

rates, and fission fragment distribution on the radioactive heating and kilonova emissions by mass outflows from NSMs have been investigated as well (Zhu et al., 2021; Barnes et al., 2021).

Here, we focus on neutron-capture rates and explore the impact of their variation for a range of initial astrophysical conditions typical of NSM ejecta. In particular, we study r-process nucleosynthesis in material that is either dynamically ejected during the merger of BNS [see also Mumpower et al. (2016), and references therein] or after the merger in the form of wind outflows over longer timescales. For the set of astrophysical trajectories considered, we perform a sensitivity study by changing single n-capture rates. We identify the nuclides that mostly affect the r-process abundance pattern and produce the larger variations in the total energy released by the decay of r-process elements. Finally, the inventory of isotopes and elements with the highest sensitivity to single n-capture rate changes is presented.

2 Methods

We make use of the freely available nuclear network code `SkyNet` (Lippuner and Roberts, 2017), which includes more than 7,000 isotopes up to Cn. We adopt the same setup used in Perego et al. (2022), except for the strong and weak nuclear reactions, for which we employ the latest default version of the JINA REACLIB library (from 06/20/2021).

We have performed r-process calculations for a NSM scenario. In particular, five parameterized fluid trajectories are considered, representative of the conditions in initial electron fraction (Y_e[1]), initial entropy (s), and expansion timescale (τ), within the material from the dynamical ejecta (both at polar and equatorial angles (Radice et al., 2018; Bernuzzi et al., 2020; Perego et al., 2022), the spiral-wave wind ejecta (Nedora et al., 2019, 2021), the neutrino-driven wind ejecta (Perego et al., 2014; Martin et al., 2015), and the viscosity-driven wind ejecta (Fernández and Metzger, 2013; Just et al., 2015; Wu et al., 2016). Specifically, we adopted the following (Y_e, s [k_B baryon^{-1}], τ [ms]) combinations:

- (0.05, 8, and 10) for the dynamical ejecta at equatorial latitudes
- (0.35, 30, and10) for the dynamical ejecta at polar latitudes
- (0.30, 20, and 10) for the spiral-wave wind ejecta
- (0.35, 15, and 30) for the ν-driven disk wind ejecta
- (0.25, 20, and 80) for the viscous ejecta

In the following, we will refer to these models as DynEq, DynPo, SpiWW, DisWN, and DisWV, respectively. All the trajectories are initialized in nuclear statistical equilibrium (NSE) conditions at $T_0 = 6$ GK. The initial density is accordingly determined from solving for NSE at the given Y_e and s. The subsequent evolution is then set to follow an initially exponentially decreasing profile with time ($\rho \propto e^{-t/\tau}$), smoothly switching to a homologous expansion ($\rho \propto t^{-3}$) at $t = 3\tau$ (Lippuner and Roberts, 2015; Perego et al., 2022). The temperature is evolved accounting for the heating from nuclear reactions [e.g., Freiburghaus et al. (1999)]. To obtain the final abundances, the nuclear reaction network is evolved up to 10 Myr. Figure 1 shows the final abundance pattern obtained for the chosen astrophysical trajectories. Their comparison with the solar r-process residuals shows that the ensemble of trajectories is able to approximately reproduce all the data range up to the heaviest nuclei. Specifically, the DynEq ejecta produces a full r-process pattern, inclusive of the second and third r-process peak elements, whose relative abundances are close to solar ones. Actinides are significantly produced as well. DynPo, SpiWW, and DisWN ejecta do instead lead to a weak r-process, being only the light r-process elements to be synthesized. The DisWV case extends up to the second r-process peak but does not produce lanthanides. These simulations served as a baseline for the sensitivity study. The latter was performed by first varying a single neutron-capture rate and then recomputing a new simulation, whose predictions for the final abundance patterns were compared with the baseline ones. (n, γ) rates were individually changed by either multiplying or dividing by a constant factor. Since current theoretical compilations of neutron-capture rates are discrepant by two to three orders of magnitudes, a representative factor of 100 was considered [see Mumpower et al. (2016), and references therein]. The sensitivity study calculations were restricted to those rates whose target nuclei reach an abundance of at least $Y = 10^{-10}$ at any time step of the baseline simulation and have a half-life larger than 1 s, according to the evaluated data of NUBASE 2020 (Kondev et al., 2021). We further restrict the selection on those isotopes with a charge number $Z \geq 20$, since the lighter nuclei are scarcely synthesized, except hydrogen and helium, whose production is not influenced by neutron-capture rates (Perego et al., 2022). This procedure allows us to focus on those rates that may have the greatest impact on the final r-process abundance pattern and have a good chance to be measured by future experiments and, at the same time, avoid performing a massive number of simulations. The number of changed neutron-capture rates varies from ~ 300 for the ν-driven disk wind ejecta trajectory up to more than 800 for the case of equatorial dynamical ejecta trajectory.

3 Results and discussion

In Figures 2, 3, we show the results of the study for all the considered outflows from NSM. The bands represent the

1 The electron fraction is defined as the ratio between net density of electrons and the total baryon number density.

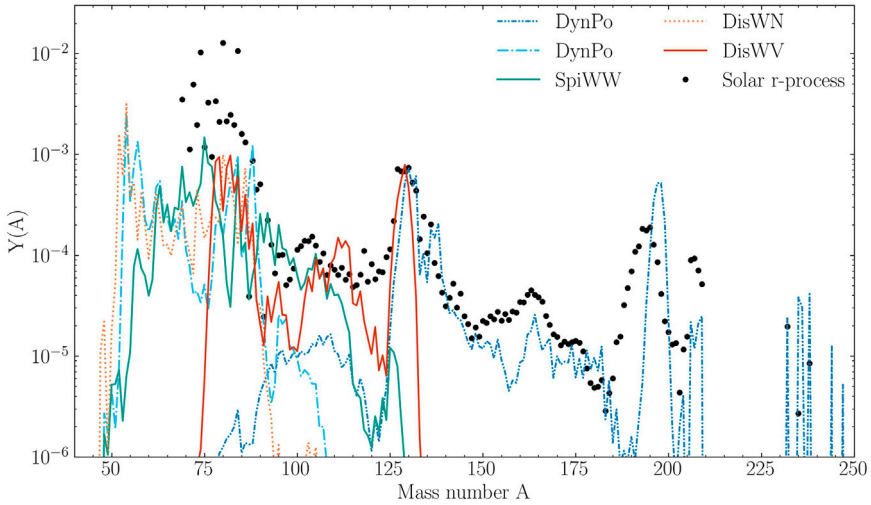

FIGURE 1
Final abundances *Y(A)* versus mass number *A* for the five parameterized baseline astrophysical trajectories representative of the different NSM ejecta channels described in the text: matter dynamically ejected during the merger at equatorial (DynEq) and polar (DynPo) angles (blue and cyan lines, respectively), and winds expelled after the merger due to the propagation of spiral arms in the NS remnant (SpiWW; green line), neutrino irradiation (DisWN; orange line), and viscous processes (DisWV; red line). The scaled solar r-residuals, obtained by multiplying the solar system abundances of Lodders (2021) by the r-fractions from Prantzos et al. (2020), are shown for comparison.

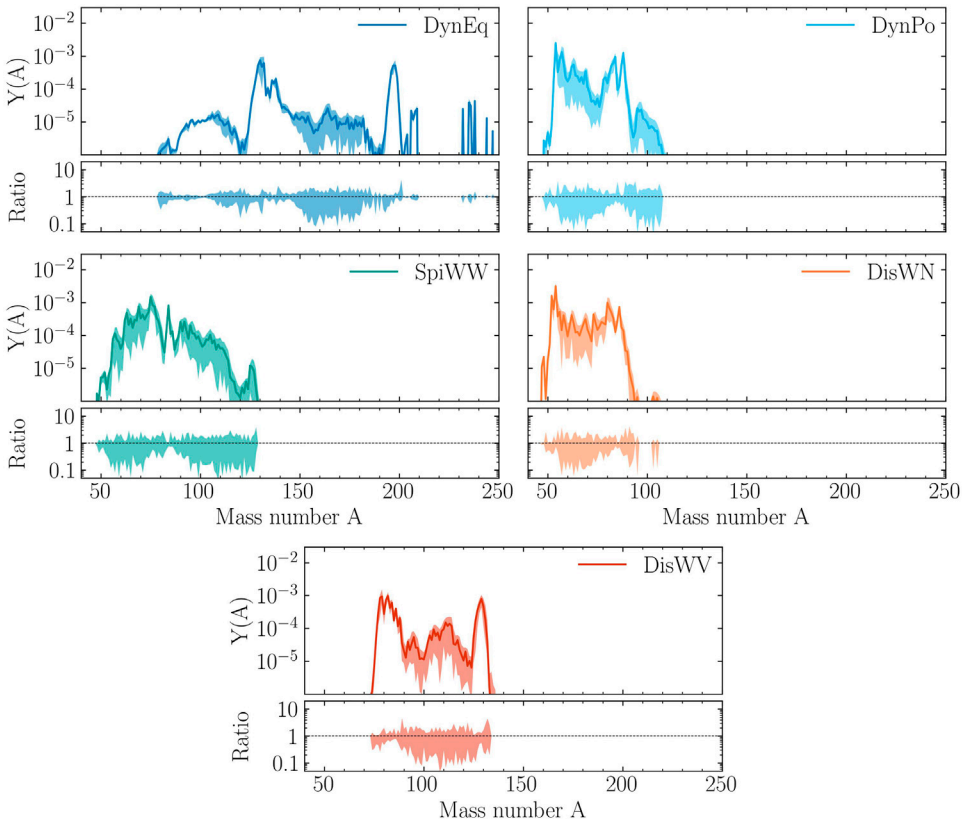

FIGURE 2
Upper panels: Variance in the isotopic abundance patterns (shaded bands), corresponding to the sensitivity studies for the different chosen trajectories. Lower panels: Ratio of final abundances with respect to the baseline. Color code as shown in Figure 1.

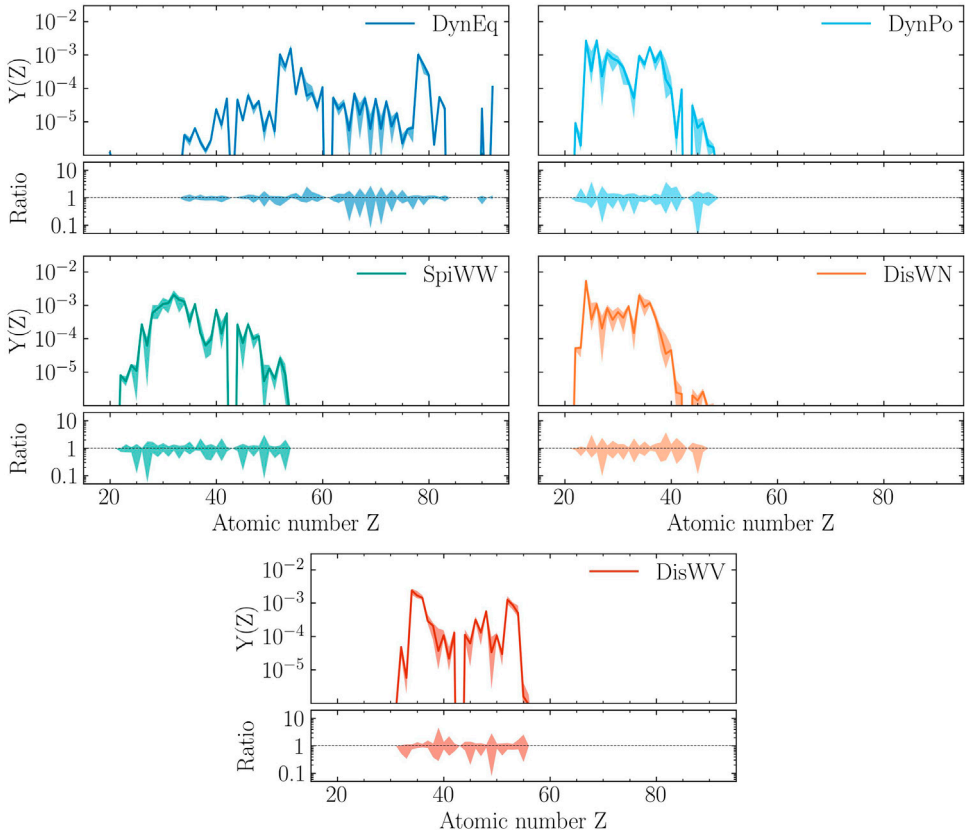

FIGURE 3
Same as shown in Figure 2 but for elemental abundances.

variance in the final abundances from changing individual (n, γ) rates of a factor of 100. The importance of neutron captures is clearly demonstrated as they produce significant variations, up to one order of magnitude, in the overall abundance pattern. For each trajectory, n-capture rates become important at the freeze-out, when β-decays take over and the r-process path moves toward stability (Surman et al., 1997). This happens later in time in the more neutron-rich ejecta due to the higher-attained neutron-to-seed ratio. During this phase, the final r-process abundance pattern is affected by both an early-freeze-out photodissociation effect and a late-freeze-out neutron capture effect (Surman et al., 2009). If the temperatures are sufficiently high, the photodissociation of abundant nuclei, populated through neutron capture, can still be efficient and the r-process path can move back to lower mass numbers, so making available further neutrons to be captured and modifying the nucleosynthesis path. When instead, as the temperature is decreasing, the r-process path shifts toward stability, late-time neutron captures are effective and compete with β-decays, possibly altering the neutron density and the β-decay pathways of the most abundant nuclei, especially of the closed-shell nuclei.

In turn, these effects also influence the radioactive energy generation rate per unit mass, $\epsilon(t)$, from the various decay channels: β-decay, α-decay, and spontaneous fission of heavy nuclei (Li and Paczyński, 1998; Metzger et al., 2010; Zhu et al., 2018; Wu et al., 2019; Hotokezaka and Nakar, 2020).

Figure 4 shows the fluctuations induced by changing the neutron-capture rates for the various trajectories in the heating rate $\epsilon(t)$. The latter is well represented by a power law as a function of the time, even if the actual shape depends on the ejecta composition and therefore on the initial Y_e (Lippuner and Roberts, 2015; Wanajo, 2018). In general, noteworthy variations are found for all the considered case studies and in particular for the high-Y_e ejecta ones. DynPo, SpiWW, and DisWN models do, in fact, produce a considerable amount of nuclei only in the limited range $50 \lesssim A \lesssim 90$, where very few isotopes have half-lives of 10–100 days that may produce marked features in bolometric kilonova lightcurves (Wu et al., 2019).

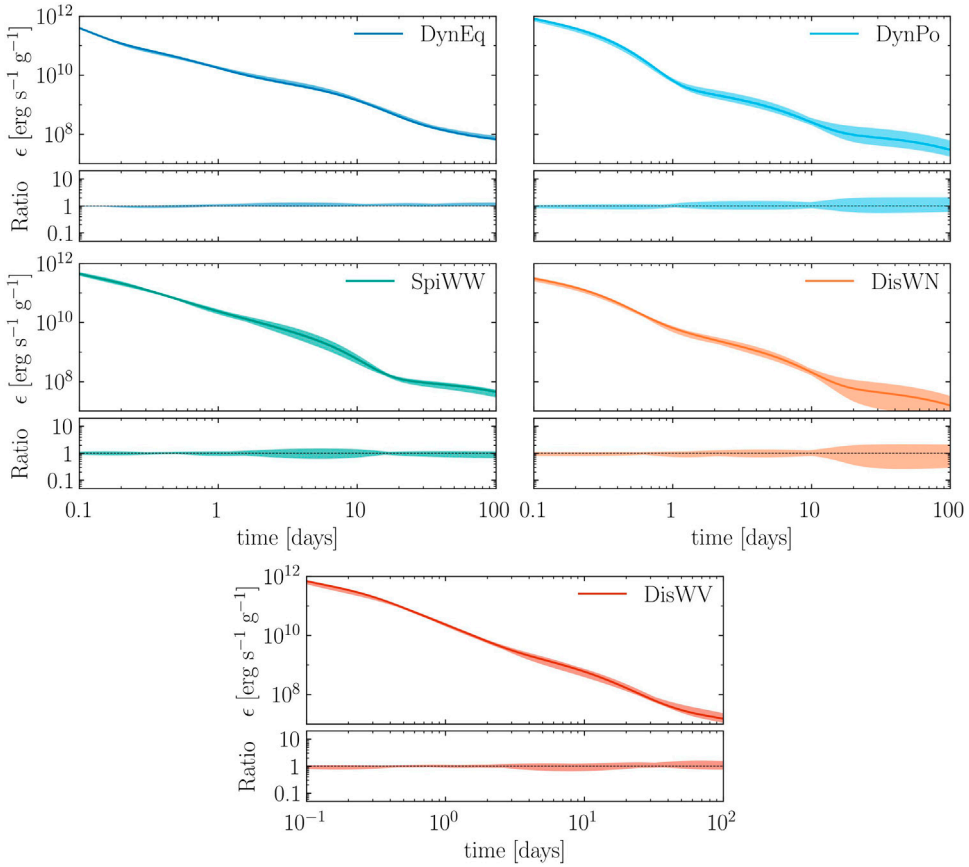

FIGURE 4
Upper panels: Variance in the nuclear heating rate (shaded bands), corresponding to the sensitivity studies for the different chosen trajectories, in the time window 0.1–100 days. Lower panels: Ratio of the heating rate with respect to the baseline. Color code as shown in Figure 1.

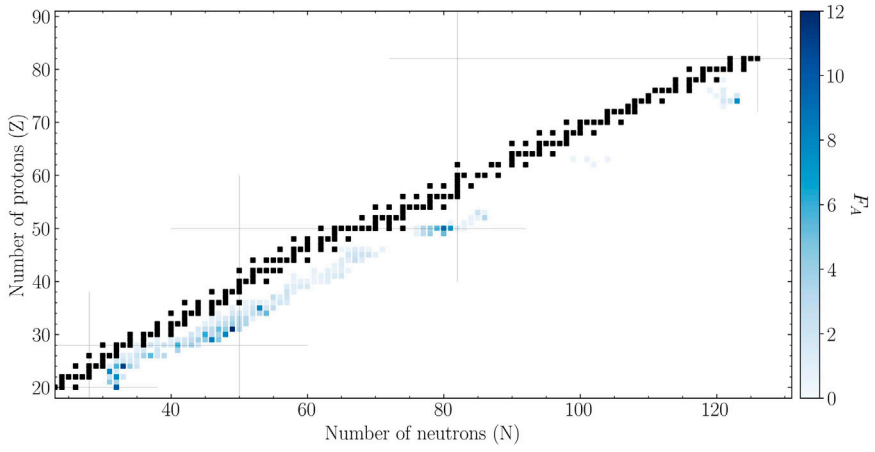

FIGURE 5
Combined results of all neutron-capture rate sensitivity studies performed. The shading represents the sensitivity measure F_A. Only nuclei with sensitivity values F_A greater than 0.5 in at least one of considered astrophysical trajectories are shaded. Black squares denote stable nuclei.

TABLE 1 Top 30 nuclei with maximum neutron-capture rate sensitivity measure F_A for the five NSM ejecta trajectories considered in this study. For each specific nucleus, the relative F_A value is the largest one obtained in the full set of sensitivity studies and refers to the particular type of ejecta listed.

Z	A	Element	F_A	Ejecta
31	80	Ga	12.16	DisWN
24	57	Cr	11.13	DynPo
20	52	Ca	9.74	DisWN
50	130	Sn	9.06	DynEq
29	75	Cu	8.52	SpiWW
35	88	Br	8.08	DynPo
30	78	Zn	7.98	DisWV
23	54	V	7.74	DisWN
22	54	Ti	7.62	DisWN
74	197	W	7.51	DynEq
50	131	Sn	7.11	DynEq
30	75	Zn	6.12	SpiWW
28	69	Ni	5.68	SpiWW
24	56	Cr	5.60	DynPo
50	129	Sn	5.56	DisWV
34	88	Se	5.28	DynPo
26	63	Fe	5.25	DynPo
49	129	In	5.20	DisWV
31	78	Ga	5.11	DisWV
29	76	Cu	4.52	SpiWW
21	52	Sc	4.34	DisWN
29	74	Cu	4.30	SpiWW
50	128	Sn	4.12	DisWV
24	58	Cr	4.12	DynPo
31	79	Ga	4.08	DisWV
49	127	In	4.02	DisWV
32	81	Ge	3.81	DisWN
29	73	Cu	3.79	DisWN
28	71	Ni	3.70	SpiWW
26	62	Fe	3.69	DynPo

TABLE 2 Top 30 nuclei with maximum nuclear heating rate sensitivity measure D_t (see text for details). The maximum value attained at any time t = 0.1, 1, 10, 100 days is set in boldface. For each specific nucleus, the relative D_t value is the largest one obtained in the full set of sensitivity studies and refers to the particular type of ejecta listed.

Z	A	Element	D_{-1}	D_0	D_{+1}	D_{+2}	Ejecta
35	88	Br	12.53	8.98	24.79	**67.83**	DynPo
24	58	Cr	0.08	0.49	16.44	**57.03**	DisWN
24	59	Cr	0.21	0.58	13.17	**44.23**	DisWN
34	88	Se	8.81	5.24	14.60	**41.40**	DynPo
25	59	Mn	0.15	0.37	8.87	**30.49**	DisWN
25	58	Mn	0.05	0.20	7.57	**26.14**	DisWN
41	106	Nb	0.09	0.47	0.31	**24.16**	DisWV
28	71	Ni	0.46	7.98	**23.90**	0.04	SpiWW
37	94	Rb	0.10	0.07	0.94	**21.50**	DisWV
28	65	Ni	0.50	11.09	**20.10**	2.08	DynPo
26	65	Fe	1.04	10.20	**19.57**	1.90	DynPo
38	95	Sr	0.17	0.45	2.28	**19.48**	SpiWW
29	72	Cu	1.47	5.60	**18.97**	0.20	SpiWW
49	127	In	0.36	6.47	**18.73**	1.05	DisWV
26	59	Fe	0.00	0.23	5.06	**17.11**	DisWN
74	197	W	0.88	4.28	0.66	**17.10**	DynEq
50	127	Sn	0.26	5.80	**15.41**	1.10	DisWV
27	65	Co	0.50	8.27	**15.36**	1.75	DynPo
30	77	Zn	4.28	**14.18**	2.79	0.76	DisWN
30	78	Zn	**14.08**	0.76	1.07	0.69	DisWV
28	72	Ni	0.83	3.94	**13.95**	0.04	SpiWW
50	130	Sn	0.91	1.07	**13.46**	0.83	DisWV
50	131	Sn	5.41	9.47	**13.41**	1.93	DynEq
31	77	Ga	3.98	**12.89**	2.53	0.68	DisWN
49	126	In	1.93	1.82	**12.86**	0.96	DisWV
42	105	Mo	0.24	0.59	0.33	**12.42**	DisWV
29	71	Cu	0.35	3.68	**11.93**	0.17	SpiWW
29	76	Cu	2.76	**11.83**	2.14	0.19	SpiWW
35	90	Br	1.46	4.42	2.25	**11.04**	SpiWW
24	56	Cr	**10.96**	1.84	0.67	2.17	DisWN

In the sensitivity study, for each new simulation, the impact of changing an individual neutron-capture rate on the final abundance pattern is quantified with a sensitivity measure, F_A, that is suited to estimate the *global* changes arising both from large local variations and small variations along the abundance pattern (Surman et al., 2009; Mumpower et al., 2016); it is defined as follows:

$$F_A = 100 \sum_A |X(A) - X_b(A)|, \quad (1)$$

where $X(A) = A \cdot Y(A)$ are final mass fractions of the simulation with the rate varied, and $X_b(A)$ are the final mass fractions for the baseline abundance pattern.

Given the fact that the r-process is associated with explosive events, it is not possible to have the evidence of its *in situ* nucleosynthesis with observations of stellar spectra, as instead is the case of the s-process (Käppeler et al., 2011). As a consequence, one usually looks at the solar system abundances of heavy nuclei to get information about the typical r-process abundance pattern. In particular, the r-process contribution to the solar system neutron-capture abundances is determined by subtracting the s-process contribution [e.g., Prantzos et al. (2020)]. The *residual* r-process pattern provides an extremely useful benchmark for comparing abundance predictions of r-process simulations at an

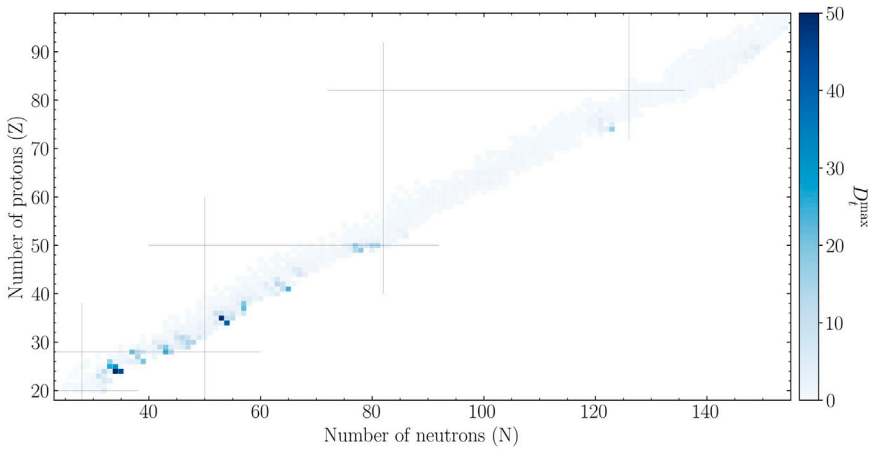

FIGURE 6
Nuclear heating rate sensitivity across the nuclear chart. For each nucleus, the shading represents the maximum sensitivity measure D_t attained at any time t = 0.1, 1, 10, 100 days.

TABLE 3 30 most sensitive elements with the relative maximum local sensitivity (F_Z^{max}) and the top three ^{A}X (n, γ) reactions with the strongest local sensitivities (F_Z) for the considered ejecta trajectory. For each element, the trajectory was selected as the one predicting the maximum abundance $Y_b^{max}(Z)$ for the baseline simulation.

Z	Element	F_Z^{max}	^{A}X	F_Z	^{A}X	F_Z	^{A}X	F_Z	$Y_b^{max}(Z)$	Ejecta
39	Y	177.29	^{88}Br	177.29	^{88}Se	106.35	^{89}Br	36.22	1.86e-04	DynPo
49	In	140.55	^{114}Rh	107.53	^{114}Pd	99.10	^{115}Rh	92.42	3.33e-05	DisWV
69	Tm	134.40	^{168}Tb	102.00	^{169}Tb	65.22	^{168}Gd	59.39	6.08e-06	DynEq
25	Mn	133.15	^{54}V	113.65	^{54}Ti	110.27	^{55}Ti	35.05	3.77e-04	DisWN
27	Co	128.21	^{58}Cr	89.84	^{59}Cr	58.98	^{58}Mn	43.58	2.27e-04	DynPo
71	Lu	119.45	^{174}Ho	87.56	^{175}Er	49.12	^{174}Dy	46.23	6.12e-06	DynEq
67	Ho	102.26	^{164}Eu	83.18	^{165}Eu	55.94	^{165}Gd	36.18	1.63e-05	DynEq
41	Nb	99.96	^{92}Rb	77.88	^{92}Kr	47.73	^{93}Kr	45.61	1.41e-04	SpiWW
57	La	95.30	^{138}I	95.30	^{138}Te	41.41	^{139}I	21.66	5.96e-05	DynEq
73	Ta	86.21	^{180}Tm	59.38	^{181}Tm	41.54	^{180}Er	37.87	7.14e-06	DynEq
65	Tb	83.96	^{158}Pm	60.36	^{159}Pm	58.52	^{159}Sm	44.47	5.44e-06	DynEq
75	Re	66.96	^{184}Lu	49.33	^{184}Yb	42.14	^{186}Lu	41.73	2.21e-06	DynEq
45	Rh	65.59	^{103}Zr	54.05	^{103}Nb	46.08	^{103}Mo	43.42	7.40e-05	SpiWW
37	Rb	44.22	^{84}As	24.59	^{87}Se	24.50	^{87}Br	13.88	6.05e-04	DynPo
77	Ir	43.59	^{193}W	33.80	^{192}Ta	13.26	^{193}Re	12.43	6.39e-06	DynEq
47	Ag	42.59	^{109}Ru	34.62	^{108}Tc	26.80	^{106}Nb	24.51	1.30e-04	DisWV
33	As	42.31	^{75}Cu	32.60	^{75}Zn	22.25	^{74}Cu	15.96	1.48e-03	SpiWW
58	Ce	41.80	^{138}Te	41.80	^{139}I	11.55	^{142}Cs	11.16	7.17e-05	DynEq
30	Zn	40.07	^{69}Ni	29.33	^{68}Co	19.42	^{65}Fe	17.89	1.09e-03	SpiWW
51	Sb	39.99	^{120}Ag	33.71	^{121}Cd	30.20	^{123}Cd	17.57	2.96e-05	DisWV
63	Eu	39.21	^{152}Pr	25.57	^{151}Pr	19.40	^{150}Pr	17.59	2.36e-05	DynEq
29	Cu	38.97	^{63}Fe	29.43	^{65}Fe	24.10	^{65}Co	14.14	8.03e-04	SpiWW
28	Ni	37.78	^{63}Fe	26.19	^{62}Fe	17.49	^{59}Cr	11.00	1.11e-03	DynPo
31	Ga	36.15	^{69}Ni	27.58	^{71}Ni	19.32	^{68}Co	17.46	1.18e-03	SpiWW
59	Pr	35.37	^{138}Te	26.43	^{141}Xe	18.89	^{139}I	14.53	2.66e-05	DynEq
23	V	31.79	^{52}Ca	29.10	^{51}Sc	9.48	^{50}Ca	8.31	5.27e-05	DisWN
38	Sr	31.54	^{88}Br	26.48	^{88}Se	18.94	^{87}Se	11.81	1.24e-03	DynPo
79	Au	30.96	^{197}W	28.44	^{196}W	7.37	^{197}Os	3.70	5.18e-04	DynEq
55	Cs	30.56	^{132}Sn	49.20	^{132}Sb	24.46	^{133}Sb	5.67	6.65e-05	DynEq
90	Th	30.26	^{232}Fr	25.54	^{236}Ac	11.95	^{231}Rn	10.21	2.45e-05	DynEq

TABLE 4 30 most sensitive isotopes with the relative maximum local sensitivity ($F_{Z,A}^{\max}$) and the top three ^{A}X (n, γ) reactions with the strongest local sensitivities ($F_{Z,A}$) for the considered ejecta trajectory. For each isotope, the trajectory was selected as the one predicting the maximum abundance $Y_{\mathrm{b}}^{\max}(Z,A)$ for the baseline simulation.

Z	A	Element	$F_{Z,A}^{\max}$	^{A}X	$F_{Z,A}$	^{A}X	$F_{Z,A}$	^{A}X	$F_{Z,A}$	$Y_{\mathrm{b}}^{\max}(Z,A)$	Ejecta
80	201	Hg	181.92	^{200}Ir	171.29	^{200}Os	24.70	^{201}Os	15.54	2.06e-06	DynEq
39	89	Y	177.29	^{88}Br	177.29	^{88}Se	106.35	^{89}Br	36.22	1.86e-04	DynPo
50	122	Sn	145.15	^{121}Cd	122.07	^{121}In	38.58	^{122}Cd	34.74	7.21e-06	DisWV
49	115	In	140.55	^{114}Rh	107.53	^{114}Pd	99.10	^{115}Rh	92.42	3.33e-05	DisWV
75	187	Re	138.45	^{186}Lu	111.44	^{187}Lu	51.34	^{186}Ta	47.35	8.28e-07	DynEq
69	169	Tm	134.40	^{168}Tb	102.00	^{169}Tb	65.22	^{168}Gd	59.39	6.08e-06	DynEq
25	55	Mn	133.15	^{54}V	113.65	^{54}Ti	110.27	^{55}Ti	35.05	3.77e-04	DisWN
28	64	Ni	131.61	^{63}Fe	109.64	^{64}Fe	45.75	^{63}Co	32.43	2.58e-04	DynPo
26	58	Fe	130.02	^{57}Cr	106.97	^{58}Cr	43.75	^{58}Mn	17.24	6.36e-04	DynPo
30	70	Zn	130.01	^{69}Ni	95.19	^{70}Ni	43.38	^{70}Cu	24.47	3.36e-04	SpiWW
27	59	Co	128.21	^{58}Cr	89.84	^{59}Cr	58.98	^{58}Mn	43.58	2.27e-04	DynPo
71	175	Lu	119.45	^{174}Ho	87.56	^{175}Er	49.12	^{174}Dy	46.23	6.12e-06	DynEq
50	120	Sn	117.34	^{120}Ag	117.34	^{119}Cd	72.84	^{119}Ag	34.59	1.05e-05	DisWV
50	118	Sn	115.88	^{117}Pd	89.52	^{117}Ag	60.00	^{118}Ag	51.69	2.24e-05	DisWV
40	94	Zr	110.77	^{94}Rb	110.77	^{93}Rb	48.52	^{93}Kr	33.38	7.98e-05	SpiWW
42	96	Mo	110.22	^{95}Sr	75.73	^{96}Y	50.93	^{96}Sr	36.38	1.17e-04	SpiWW
75	185	Re	109.42	^{184}Lu	78.88	^{184}Yb	66.46	^{185}Yb	39.70	1.38e-06	DynEq
46	108	Pd	106.84	^{108}Tc	106.84	^{107}Mo	46.12	^{107}Tc	43.31	4.34e-05	DisWV
64	155	Gd	105.97	^{154}Pr	81.89	^{155}Nd	54.25	^{155}Pr	50.45	9.20e-06	DynEq
40	91	Zr	105.79	^{90}Br	86.51	^{91}Kr	37.92	^{90}Kr	21.04	1.34e-04	SpiWW
64	157	Gd	105.20	^{156}Pm	74.56	^{157}Pm	60.53	^{157}Nd	46.81	4.52e-06	DynEq
67	165	Ho	102.26	^{164}Eu	83.18	^{165}Eu	55.94	^{165}Gd	36.18	1.63e-05	DynEq
50	124	Sn	101.24	^{123}Cd	64.60	^{124}In	62.49	^{123}In	53.62	6.37e-06	DisWV
41	93	Nb	99.96	^{92}Rb	77.88	^{92}Kr	47.73	^{93}Kr	45.61	1.41e-04	SpiWW
40	93	Zr	99.89	^{92}Rb	77.88	^{92}Kr	47.74	^{93}Kr	45.54	2.26e-06	SpiWW
50	119	Sn	99.51	^{118}Ag	64.01	^{119}Ag	53.60	^{119}Cd	50.95	1.52e-05	DisWV
30	66	Zn	96.61	^{65}Fe	84.34	^{65}Ni	62.85	^{65}Co	57.22	1.72e-04	SpiWW
46	106	Pd	96.44	^{106}Nb	96.44	^{105}Mo	52.57	^{105}Nb	47.08	5.87e-05	DisWV
72	179	Hf	95.40	^{178}Tm	64.18	^{179}Er	51.23	^{178}Er	40.31	7.34e-06	DynEq
57	139	La	95.30	^{138}I	95.30	^{138}Te	41.41	^{139}I	21.66	5.96e-05	DynEq

isotopic level (see Figure 2). However, a growing number of stellar abundance observations of very metal-poor stars showed that the solar r-process pattern is not universal and that a star-to-star scatter for *elemental* abundance distributions is present [e.g., Sneden et al. (2008); Cowan et al. (2021), and references therein]. The results of our study shown in Figure 3 demonstrate that changes in neutron-capture rates have an impact on elemental abundances as well. In order to quantify such uncertainties, a second sensitivity measure is adopted, F_Z, which is appropriate to describe local changes to individual elements by single neutron-capture rate variations, and it is defined as follows:

$$F_Z = 100\ \frac{|Y(Z) - Y_{\mathrm{b}}(Z)|}{Y_{\mathrm{b}}(Z)}. \tag{2}$$

Analogously, to describe local changes to individual isotopes, we define $F_{Z,A}$ as follows:

$$F_{Z,A} = 100\ \frac{|Y(Z,A) - Y_{\mathrm{b}}(Z,A)|}{Y_{\mathrm{b}}(Z,A)}. \tag{3}$$

To describe the variations in the nuclear decay heating rate $\epsilon(t)$ at a time t, we introduce another sensitivity measure, D_t, which is defined as follows:

$$D_t = 100\ \frac{|\epsilon(t) - \epsilon_{\mathrm{b}}(t)|}{\epsilon_{\mathrm{b}}(t)}. \tag{4}$$

The final sensitivity measures F_A, F_Z, $F_{Z,A}$, and D_t are computed as an average between the values obtained considering the case where a single neutron-capture rate is increased and decreased by a factor of 100.

Figure 5 and Table 1 show the nuclei with the greatest sensitivity F_A obtained in the full set of studies. Regardless of the different astrophysical trajectories considered, the nuclei having the greatest influence on the r-process in NSM scenarios are those located across the neutron closed-shell regions [see also Mumpower et al. (2016), and references therein]. In particular, depending on the considered shell, we can individuate different subsets. In the $N = 50$ region, neutron-rich isotopes of copper, zinc, gallium, selenium, and bromine show the highest impact. Cadmium, indium, tin, and tungsten isotopes are the most important in $N = 82$, 126 regions. When considering trajectories with high electron fraction ($Y_e = 0.35$), also neutron-rich isotopes in the vicinity of $N = 28$ zone, of elements such as calcium, titanium, vanadium, and chromium, affect r-process abundance distribution.

We note that these nuclei exhibit large effects on the r-process nucleosynthesis in NSMs, as the five sets of astrophysical trajectories considered for the studies are representative of a NSM scenario. In principle, other nuclei may be important as well in other r-process scenarios. Nonetheless, determination of these n-capture cross sections should be of top priority in measurement campaigns at current and future exotic RIB facilities, given that NSMs are acknowledged to be an r-process site, even if other sources might be needed to explain the r-process enrichment in the Universe [e.g., Côté et al. (2019); Skúladóttir et al. (2019); Van der Swaelmen et al. (2022)].

In Table 2, the nuclei with the greatest sensitivity D_t at different considered times are listed. In particular, each D_i refers to a time equal to $t = 10^i$ days. So, for example, D_0 is the sensitivity to a specific neutron-capture rate for the radioactive heating rate at 1 day. It is straightforward noticing that the effect of varying the neutron-capture rates on the nuclear decay heating rate is somewhat milder, being within a factor of ~ 5. Nonetheless, a few reaction rates produce noticeable variations for high-Y_e ejecta at relatively late times ($t \gtrsim 10$ days). This is due to the fact that the radioactive energy generation is dominated by a few nuclei that can decay on timescales greater than some days and have half-lives ($t_{1/2}$) comparable to t (Wu et al., 2019). A clear example is represented by ^{89}Sr, which has a half-life of 50.563 days. Its production is sensitive to the amount of the parent isobars, e.g., ^{89}Br and ^{89}Se, which in turn depend on the neutron-capture reaction rate on ^{88}Br and ^{88}Se. Thus, a substantial change in these rates alters the r-process path leading to the production of ^{89}Sr and consequently its β-decay contribution to the heating rate.

We note that nuclei with larger D_t measures are located just on the right of $N = 28$ and $N = 50$ regions of the nuclear chart (see Figure 6).

Depending on the production site, special isotopes or elements can be of interest in nuclear astrophysics, e.g., because they can be measured in solar system material or detected in stellar spectra. In this regard, it is useful also to evaluate which of them are mostly affected by neutron-capture rate variations and the rates responsible for that. The most sensitive elements to n-capture rate variations are listed in Table 3. The maximum local sensitivity, $F_Z^{\max}$, is computed as follows

$$F_Z^{\max} = 100\ \frac{\left|Y^{\max}(Z) - Y^{\min}(Z)\right|}{Y_b(Z)}, \tag{5}$$

where $Y^{\max}(Z)$ is the abundance at the top of the uncertainty band for atomic number Z, and $Y^{\min}(Z)$ is the one at the bottom (see Figure 3). The top three rates that have the biggest effects on individual elements are indicated as well. Similarly, the isotopes whose abundance is most affected by the changes in the neutron-capture rates are shown in Table 4. Their maximum local sensitivity, $F_{Z,A}^{\max}$, are computed as in Equation 5 but considering isotopic abundances $Y(Z,A)$. Note that the elements (isotopes) with $F_Z = F_Z^{\max}$ ($F_{Z,A} = F_{Z,A}^{\max}$) dominate the uncertainty and completely determine the final abundance of the specific element (isotope) under consideration.

4 Conclusions

The impact of neutron-capture rate uncertainties on the r-process in neutron star mergers has been systematically studied for five different astrophysical trajectories representative of various ejecta channels from NSMs. We investigated the sensitivity of the relative r-process abundance yields, focusing on the capture rates of relatively long-lived nuclei. In accordance with prior studies (Surman et al., 2009; Mumpower et al., 2012, 2016), we found that the most significant n-capture rates are those involving nuclei located in the vicinity of neutron-closed shells $N = 50$, 82, 126, while for high-Y_e ejecta, isotopes in the $N = 28$ region considerably influence the final abundance pattern as well.

Rate variations also affects the nuclear heating rate at timescales relevant for the kilonova emission, especially at late times ($t \gtrsim 10$ days) and for high-Y_e trajectories, where a few nuclei with a comparable β-decay lifetimes contribute the most to the heating.

Finally, the most sensitive isotopes and elements to n-capture rate changes were determined and listed, along with the rates that largely influence their production. The results presented in this study can be used as guidance to prioritize future experimental campaigns for the determination of neutron-capture rate reaction of interest for the r-process occurring in NSMs.

Data availability statement

The raw data supporting the conclusions of this article will be made available by the authors, without undue reservation.

Author contributions

DV and RR conceptualized the study. DV performed the simulations and carried out the analysis. DV took care of the original draft preparation. All authors contributed to the review and editing of the manuscript and approved the submitted version.

Funding

AC was supported by the U.S. Department of Energy through the Los Alamos National Laboratory, operated by Triad National Security, LLC, for the National Nuclear Security Administration of the U.S. Department of Energy (Contract No. 89233218CNA000001). DV was supported by the German-Israeli Foundation (GIF No. I-1500-303.7/2019).

Acknowledgments

DV thanks A. Perego, S. Giuliani, and L. Chiesa for fruitful discussions concerning the modeling of the r-process nucleosynthesis in NSMs.

Conflict of interest

The authors declare that the research was conducted in the absence of any commercial or financial relationships that could be construed as a potential conflict of interest.

Publisher's note

All claims expressed in this article are solely those of the authors and do not necessarily represent those of their affiliated organizations, or those of the publisher, the editors, and the reviewers. Any product that may be evaluated in this article, or claim that may be made by its manufacturer, is not guaranteed or endorsed by the publisher.

References

Abbott, B. P., Abbott, R., Abbott, T. D., Acernese, F., Ackley, K., Adams, C., et al. (2017a). GW170817: Observation of gravitational waves from a binary neutron star inspiral. *Phys. Rev. Lett.* 119, 161101. doi:10.1103/PhysRevLett.119.161101

Abbott, B. P., Abbott, R., Abbott, T. D., Acernese, F., Ackley, K., Adams, C., et al. (2017b). Multi-messenger observations of a binary neutron star merger. *Astrophys. J.* 848, L12. doi:10.3847/2041-8213/aa91c9

Arcavi, I., Hosseinzadeh, G., Howell, D. A., McCully, C., Poznanski, D., Kasen, D., et al. (2017). Optical emission from a kilonova following a gravitational-wave-detected neutron-star merger. *Nature* 551, 64–66. doi:10.1038/nature24291

Arcones, A., and Martínez-Pinedo, G. (2011). Dynamicalr-process studies within the neutrino-driven wind scenario and its sensitivity to the nuclear physics input. *Phys. Rev. C* 83, 045809. doi:10.1103/PhysRevC.83.045809

Arnould, M., Goriely, S., and Takahashi, K. (2007). The r-process of stellar nucleosynthesis: Astrophysics and nuclear physics achievements and mysteries. *Phys. Rep.* 450, 97–213. doi:10.1016/j.physrep.2007.06.002

Barnes, J., Zhu, Y. L., Lund, K. A., Sprouse, T. M., Vassh, N., McLaughlin, G. C., et al. (2021). Kilonovae across the nuclear physics landscape: The impact of nuclear physics uncertainties on r-process-powered emission. *Astrophys. J.* 918, 44. doi:10.3847/1538-4357/ac0aec

Bernuzzi, S., Breschi, M., Daszuta, B., Endrizzi, A., Logoteta, D., Nedora, V., et al. (2020). Accretion-induced prompt black hole formation in asymmetric neutron star mergers, dynamical ejecta, and kilonova signals. *Mon. Not. R. Astron. Soc.* 497, 1488–1507. doi:10.1093/mnras/staa1860

Ciolfi, R., and Kalinani, J. V. (2020). Magnetically driven baryon winds from binary neutron star merger remnants and the blue kilonova of 2017 august. *Astrophysical J. Lett.* 900, L35. doi:10.3847/2041-8213/abb240

Côté, B., Eichler, M., Arcones, A., Hansen, C. J., Simonetti, P., Frebel, A., et al. (2019). Neutron star mergers might not Be the only source of r-process elements in the milky way. *Astrophys. J.* 875, 106. doi:10.3847/1538-4357/ab10db

Coulter, D. A., Foley, R. J., Kilpatrick, C. D., Drout, M. R., Piro, A. L., Shappee, B. J., et al. (2017). Swope Supernova Survey 2017a (SSS17a), the optical counterpart to a gravitational wave source. *Science* 358, 1556–1558. doi:10.1126/science.aap9811

Couture, A., and Reifarth, R. (2007). Direct measurements of neutron capture on radioactive isotopes. *Atomic Data Nucl. Data Tables* 93, 807–830. doi:10.1016/j.adt.2007.06.003

Cowan, J. J., Sneden, C., Lawler, J. E., Aprahamian, A., Wiescher, M., Langanke, K., et al. (2021). Origin of the heaviest elements: The rapid neutron-capture process. *Rev. Mod. Phys.* 93, 015002. doi:10.1103/RevModPhys.93.015002

Drout, M. R., Piro, A. L., Shappee, B. J., Kilpatrick, C. D., Simon, J. D., Contreras, C., et al. (2017). Light curves of the neutron star merger GW170817/SSS17a: Implications for r-process nucleosynthesis. *Science* 358, 1570–1574. doi:10.1126/science.aaq0049

Evans, P. A., Cenko, S. B., Kennea, J. A., Emery, S. W. K., Kuin, N. P. M., Korobkin, O., et al. (2017). Swift and NuSTAR observations of GW170817: Detection of a blue kilonova. *Science* 358, 1565–1570. doi:10.1126/science.aap9580

Fernández, R., and Metzger, B. D. (2013). Delayed outflows from black hole accretion tori following neutron star binary coalescence. *Mon. Not. R. Astron. Soc.* 435, 502–517. doi:10.1093/mnras/stt1312

Freiburghaus, C., Rosswog, S., and Thielemann, F. K. (1999). [CLC] [ITAL]r[/ITAL] [/CLC]-Process in neutron star mergers. *Astrophys. J.* 525, L121–L124. doi:10.1086/312343

Fujibayashi, S., Kiuchi, K., Nishimura, N., Sekiguchi, Y., and Shibata, M. (2018). Mass ejection from the remnant of a binary neutron star merger: Viscous-radiation hydrodynamics study. *Astrophys. J.* 860, 64. doi:10.3847/1538-4357/aabafd

Gillanders, J. H., Smartt, S. J., Sim, S. A., Bauswein, A., and Goriely, S. (2022). Modelling the spectra of the kilonova AT2017gfo - I. The photospheric epochs. *Mon. Not. R. Astron. Soc.* 515, 631–651. doi:10.1093/mnras/stac1258

Hauser, W., and Feshbach, H. (1952). The inelastic scattering of neutrons. *Phys. Rev.* 87, 366–373. doi:10.1103/PhysRev.87.366

Horowitz, C. J., Arcones, A., Côté, B., Dillmann, I., Nazarewicz, W., Roederer, I. U., et al. (2019). r-process nucleosynthesis: connecting rare-isotope beam facilities with the cosmos. *J. Phys. G. Nucl. Part. Phys.* 46, 083001. doi:10.1088/1361-6471/ab0849

Hotokezaka, K., and Nakar, E. (2020). Radioactive heating rate of r-process elements and macronova light curve. *Astrophys. J.* 891, 152. doi:10.3847/1538-4357/ab6a98

Just, O., Bauswein, A., Ardevol Pulpillo, R., Goriely, S., and Janka, H. T. (2015). Comprehensive nucleosynthesis analysis for ejecta of compact binary mergers. *Mon. Not. R. Astron. Soc.* 448, 541–567. doi:10.1093/mnras/stv009

Käppeler, F., Gallino, R., Bisterzo, S., and Aoki, W. (2011). Thesprocess: Nuclear physics, stellar models, and observations. *Rev. Mod. Phys.* 83, 157–193. doi:10.1103/RevModPhys.83.157

Kasen, D., Metzger, B., Barnes, J., Quataert, E., and Ramirez-Ruiz, E. (2017). Origin of the heavy elements in binary neutron-star mergers from a gravitational-wave event. *Nature* 551, 80–84. doi:10.1038/nature24453

Kasliwal, M. M., Nakar, E., Singer, L. P., Kaplan, D. L., Cook, D. O., Van Sistine, A., et al. (2017). Illuminating gravitational waves: A concordant picture of photons from a neutron star merger. *Science* 358, 1559–1565. doi:10.1126/science.aap9455

Kondev, F. G., Wang, M., Huang, W. J., Naimi, S., and Audi, G. (2021). The NUBASE2020 evaluation of nuclear physics properties. *Chin. Phys. C* 45, 030001. doi:10.1088/1674-1137/abddae

Kullmann, I., Goriely, S., Just, O., Bauswein, A., and Janka, H. T. (2022). Extensive study of nuclear uncertainties and their impact on the r-process nucleosynthesis in neutron star mergers. *arXiv e-prints*. arXiv:2207.07421. doi:10.48550/arXiv.2207.07421

Li, L. X., and Paczyński, B. (1998). Transient events from neutron star mergers. *Astrophys. J.* 507, L59–L62. doi:10.1086/311680

Lippuner, J., Fernández, R., Roberts, L. F., Foucart, F., Kasen, D., Metzger, B. D., et al. (2017). Signatures of hypermassive neutron star lifetimes on r-process nucleosynthesis in the disc ejecta from neutron star mergers. *Mon. Not. R. Astron. Soc.* 472, 904–918. doi:10.1093/mnras/stx1987

Lippuner, J., and Roberts, L. F. (2015). r-Process lanthanide production and heating rates in kilonovae. *Astrophys. J.* 815, 82. doi:10.1088/0004-637X/815/2/82

Lippuner, J., and Roberts, L. F. (2017). SkyNet: A modular nuclear reaction network library. *Astrophys. J. Suppl. Ser.* 233, 18. doi:10.3847/1538-4365/aa94cb

Lodders, K. (2021). Relative atomic solar system Abundances, mass fractions, and atomic masses of the elements and their isotopes, composition of the solar photosphere, and compositions of the major chondritic meteorite groups. *Space Sci. Rev.* 217, 44. doi:10.1007/s11214-021-00825-8

Martin, D., Perego, A., Arcones, A., Thielemann, F. K., Korobkin, O., and Rosswog, S. (2015). Neutrino-driven winds in the aftermath of a neutron star merger: Nucleosynthesis and electromagnetic transients. *Astrophys. J.* 813, 2. doi:10.1088/0004-637X/813/1/2

Metzger, B. D. (2019). Kilonovae. *Living Rev. Relativ.* 23, 1. doi:10.1007/s41114-019-0024-0

Metzger, B. D., Martínez-Pinedo, G., Darbha, S., Quataert, E., Arcones, A., Kasen, D., et al. (2010). Electromagnetic counterparts of compact object mergers powered by the radioactive decay of r-process nuclei. *Mon. Not. R. Astron. Soc.* 406, 2650–2662. doi:10.1111/j.1365-2966.2010.16864.x

Metzger, B. D., Thompson, T. A., and Quataert, E. (2018). A magnetar origin for the kilonova ejecta in GW170817. *Astrophys. J.* 856, 101. doi:10.3847/1538-4357/aab095

Mumpower, M. R., McLaughlin, G. C., and Surman, R. (2012). Influence of neutron capture rates in the rare Earth region on ther-process abundance pattern. *Phys. Rev. C* 86, 035803. doi:10.1103/PhysRevC.86.035803

Mumpower, M. R., Surman, R., McLaughlin, G. C., and Aprahamian, A. (2016). The impact of individual nuclear properties onr-process nucleosynthesis. *Prog. Part. Nucl. Phys.* 86, 86–126. doi:10.1016/j.ppnp.2015.09.001

Nedora, V., Bernuzzi, S., Radice, D., Daszuta, B., Endrizzi, A., Perego, A., et al. (2021). Numerical relativity simulations of the neutron star merger GW170817: Long-term remnant evolutions, winds, remnant disks, and nucleosynthesis. *Astrophys. J.* 906, 98. doi:10.3847/1538-4357/abc9be

Nedora, V., Bernuzzi, S., Radice, D., Perego, A., Endrizzi, A., and Ortiz, N. (2019). Spiral-wave wind for the blue kilonova. *Astrophys. J.* 886, L30. doi:10.3847/2041-8213/ab5794

Nicholl, M., Berger, E., Kasen, D., Metzger, B. D., Elias, J., Briceño, C., et al. (2017). The electromagnetic counterpart of the binary neutron star merger LIGO/virgo GW170817. III. Optical and UV spectra of a blue kilonova from fast polar ejecta. *Astrophys. J.* 848, L18. doi:10.3847/2041-8213/aa9029

Perego, A., Radice, D., and Bernuzzi, S. (2017). AT 2017gfo: An anisotropic and three-component kilonova counterpart of GW170817. *Astrophys. J.* 850, L37. doi:10.3847/2041-8213/aa9ab9

Perego, A., Rosswog, S., Cabezón, R. M., Korobkin, O., Käppeli, R., Arcones, A., et al. (2014). Neutrino-driven winds from neutron star merger remnants. *Mon. Notices R. Astronomical Soc.* 443, 3134–3156. doi:10.1093/mnras/stu1352

Perego, A., Vescovi, D., Fiore, A., Chiesa, L., Vogl, C., Benetti, S., et al. (2022). Production of very light elements and strontium in the early ejecta of neutron star mergers. *Astrophys. J.* 925, 22. doi:10.3847/1538-4357/ac3751

Pian, E., D'Avanzo, P., Benetti, S., Branchesi, M., Brocato, E., Campana, S., et al. (2017). Spectroscopic identification of r-process nucleosynthesis in a double neutron-star merger. *Nature* 551, 67–70. doi:10.1038/nature24298

Prantzos, N., Abia, C., Cristallo, S., Limongi, M., and Chieffi, A. (2020). Chemical evolution with rotating massive star yields II. A new assessment of the solar s- and r-process components. *Mon. Not. R. Astron. Soc.* 491, 1832–1850. doi:10.1093/mnras/stz3154

Radice, D., Bernuzzi, S., and Perego, A. (2020). The dynamics of binary neutron star mergers and GW170817. *Annu. Rev. Nucl. Part. Sci.* 70, 95–119. doi:10.1146/annurev-nucl-013120-114541

Radice, D., Perego, A., Hotokezaka, K., Fromm, S. A., Bernuzzi, S., and Roberts, L. F. (2018). Binary neutron star mergers: Mass ejection, electromagnetic counterparts, and nucleosynthesis. *Astrophys. J.* 869, 130. doi:10.3847/1538-4357/aaf054

Reifarth, R., Erbacher, P., Fiebiger, S., Göbel, K., Heftrich, T., Heil, M., et al. (2018). Neutron-induced cross sections - from raw data to astrophysical rates. *Eur. Phys. J. Plus* 133, 424. doi:10.1140/epjp/i2018-12295-3

Reifarth, R., Göbel, K., Heftrich, T., Weigand, M., Jurado, B., Käppeler, F., et al. (2017). Spallation-based neutron target for direct studies of neutron-induced reactions in inverse kinematics. *Phys. Rev. Accel. Beams* 20, 044701. doi:10.1103/physrevaccelbeams.20.044701

Reifarth, R., Lederer, C., and Käppeler, F. (2014). Neutron reactions in astrophysics. *J. Phys. G. Nucl. Part. Phys.* 41, 053101. doi:10.1088/0954-3899/41/5/053101

Reifarth, R., and Litvinov, Y. A. (2014). Measurements of neutron-induced reactions in inverse kinematics. *Phys. Rev. St. Accel. Beams* 17, 014701. doi:10.1103/physrevstab.17.014701

Shibata, M., Fujibayashi, S., and Sekiguchi, Y. (2021). Long-term evolution of a merger-remnant neutron star in general relativistic magnetohydrodynamics: Effect of magnetic winding. *Phys. Rev. D.* 103, 043022. doi:10.1103/PhysRevD.103.043022

Skúladóttir, Á., Hansen, C. J., Salvadori, S., and Choplin, A. (2019). Neutron-capture elements in dwarf galaxies. I. Chemical clocks and the short timescale of the r-process. *Astron. Astrophys.* 631, A171. doi:10.1051/0004-6361/201936125

Smartt, S. J., Chen, T. W., Jerkstrand, A., Coughlin, M., Kankare, E., Sim, S. A., et al. (2017). A kilonova as the electromagnetic counterpart to a gravitational-wave source. *Nature* 551, 75–79. doi:10.1038/nature24303

Sneden, C., Cowan, J. J., and Gallino, R. (2008). Neutron-capture elements in the early galaxy. *Annu. Rev. Astron. Astrophys.* 46, 241–288. doi:10.1146/annurev.astro.46.060407.145207

Soares-Santos, M., Holz, D. E., Annis, J., Chornock, R., Herner, K., Berger, E., et al. (2017). The electromagnetic counterpart of the binary neutron star merger LIGO/virgo GW170817. I. Discovery of the optical counterpart using the dark energy camera. *Astrophys. J.* 848, L16. doi:10.3847/2041-8213/aa9059

Sprouse, T. M., Navarro Perez, R., Surman, R., Mumpower, M. R., McLaughlin, G. C., and Schunck, N. (2020). Propagation of statistical uncertainties of Skyrme mass models to simulations of r-process nucleosynthesis. *Phys. Rev. C* 101, 055803. doi:10.1103/PhysRevC.101.055803

Surman, R., Beun, J., McLaughlin, G. C., and Hix, W. R. (2009). Neutron capture rates nearA=130that effect a global change to ther-process abundance distribution. *Phys. Rev. C045809* 79. doi:10.1103/PhysRevC.79.045809

Surman, R., Engel, J., Bennett, J. R., and Meyer, B. S. (1997). Source of the rare-earth element peak inr-process nucleosynthesis. *Phys. Rev. Lett.* 79, 1809–1812. doi:10.1103/PhysRevLett.79.1809

Surman, R., Mumpower, M., Sinclair, R., Jones, K. L., Hix, W. R., and McLaughlin, G. C. (2014). Sensitivity studies for the weak r process: Neutron capture rates. *AIP Adv.* 4, 041008. doi:10.1063/1.4867191

Tanaka, M., Utsumi, Y., Mazzali, P. A., Tominaga, N., Yoshida, M., Sekiguchi, Y., et al. (2017). Kilonova from post-merger ejecta as an optical and near-Infrared counterpart of GW170817. *Publ. Astronomical Soc. Jpn.* 69, 102. doi:10.1093/pasj/psx121

Tanvir, N. R., Levan, A. J., González-Fernández, C., Korobkin, O., Mandel, I., Rosswog, S., et al. (2017). The emergence of a lanthanide-rich kilonova following the merger of two neutron stars. *Astrophys. J.* 848, L27. doi:10.3847/2041-8213/aa90b6

Van der Swaelmen, M., Viscasillas Vázquez, C., Cescutti, G., Magrini, L., Cristallo, S., Vescovi, D., et al. (2022). The gaia-ESO survey: Placing constraints on the origin of r-process elements. *arXiv e-prints*. arXiv:2207.14747. doi:10.48550/arXiv.2207.14747

Villar, V. A., Guillochon, J., Berger, E., Metzger, B. D., Cowperthwaite, P. S., Nicholl, M., et al. (2017). The combined ultraviolet, optical, and near-infrared light curves of the kilonova associated with the binary neutron star merger GW170817: Unified data set, analytic models, and physical implications. *Astrophys. J.* 851, L21. doi:10.3847/2041-8213/aa9c84

Wanajo, S. (2018). Physical conditions for the r-process. I. Radioactive energy sources of kilonovae. *Astrophys. J.* 868, 65. doi:10.3847/1538-4357/aae0f2

Watson, D., Hansen, C. J., Selsing, J., Koch, A., Malesani, D. B., Andersen, A. C., et al. (2019). Identification of strontium in the merger of two neutron stars. *nature* 574, 497–500. doi:10.1038/s41586-019-1676-3

Wollaeger, R. T., Korobkin, O., Fontes, C. J., Rosswog, S. K., Even, W. P., Fryer, C. L., et al. (2018). Impact of ejecta morphology and composition on the electromagnetic signatures of neutron star mergers. *Mon. Not. R. Astron. Soc.* 478, 3298–3334. doi:10.1093/mnras/sty1018

Wu, M. R., Barnes, J., Martínez-Pinedo, G., and Metzger, B. D. (2019). Fingerprints of heavy-element nucleosynthesis in the late-time lightcurves of kilonovae. *Phys. Rev. Lett.* 122, 062701. doi:10.1103/PhysRevLett.122.062701

Wu, M. R., Fernández, R., Martínez-Pinedo, G., and Metzger, B. D. (2016). Production of the entire range of r-process nuclides by black hole accretion disc outflows from neutron star mergers. *Mon. Not. R. Astron. Soc.* 463, 2323–2334. doi:10.1093/mnras/stw2156

Zhu, Y., Wollaeger, R. T., Vassh, N., Surman, R., Sprouse, T. M., Mumpower, M. R., et al. (2018). Californium-254 and kilonova light curves. *Astrophys. J.* 863, L23. doi:10.3847/2041-8213/aad5de

Zhu, Y. L., Lund, K. A., Barnes, J., Sprouse, T. M., Vassh, N., McLaughlin, G. C., et al. (2021). Modeling kilonova light curves: Dependence on nuclear inputs. *Astrophys. J.* 906, 94. doi:10.3847/1538-4357/abc69e